

A Branch Cut Algorithm for 180-Degree Ambiguity Resolution in 2D Vector Fields and Its Application to Single-Frame Fringe Projection Profilometry

Daichi Kitahara* and Isao Yamada†

*College of Information Science and Engineering, Ritsumeikan University, Kusatsu, Shiga, Japan

†Department of Information and Communications Engineering, Tokyo Institute of Technology, Meguro, Tokyo, Japan

Abstract—The 180-degree ambiguity resolution is an estimation problem of correct signs of discrete samples of a two-dimensional (2D) vector field. To estimate the correct signs at 2D lattice points, several optimization approaches are proposed. These approaches assume that the true vector field changes smoothly between many neighboring lattice points, and solve a combinatorial optimization problem on sign matrices, where the objective function is given by the sum of costs for neighboring signs. This objective function is non-submodular, and hence the optimization problem is NP-hard. For this NP-hard problem, we propose a branch cut type solver which is inspired by Goldstein’s approach for 2D phase unwrapping. In application to single-frame fringe projection profilometry, we show the effectiveness of the proposed branch cut algorithm.

I. INTRODUCTION

Suppose that discrete samples of a vector field are observed at two-dimensional (2D) lattice points (i, j) ($i = 1, 2, \dots, m$ and $j = 1, 2, \dots, n$) as $\mathbf{v}_{i,j} \in \mathcal{V}$, but each sample has the sign ambiguity, i.e., the true vector value at (i, j) is $\mathbf{v}_{i,j}$ or $-\mathbf{v}_{i,j}$. Here, \mathcal{V} is the space where $\mathbf{v}_{i,j}$ is defined, and we assume that the observation error except for the sign ambiguity is removed in advance. Such situations sometimes arise in measurements of *wind stress* [1], [2], *photospheric magnetic* [3]–[5], *in-plane displacement* [6]–[8], *unwrapped phase gradient* [9]–[17], and *color line* [18], [19] fields. This sign ambiguity is often called “the 180-degree ambiguity” because $-\mathbf{v}_{i,j}$ is given by the 180-degree rotation of $\mathbf{v}_{i,j}$ on the 2D plane if $\mathcal{V} \subset \mathbb{R}^2$.

In this paper, along the optimization approaches in [4], [5], [12]–[19], we resolve the 180-degree ambiguity via the following combinatorial optimization problem on sign matrices.

Problem 1 (A Combinatorial Optimization Problem on Sign Matrices for 180-Degree Ambiguity Resolution): Find a binary sign matrix $\mathbf{S}^* := (s_{i,j}^*) \in \{-1, +1\}^{m \times n}$ which minimizes

$$J(\mathbf{S}) := \sum_{i=1}^m \sum_{j=1}^{n-1} J_{i,j}^h(s_{i,j}, s_{i,j+1}) + \sum_{i=1}^{m-1} \sum_{j=1}^n J_{i,j}^v(s_{i,j}, s_{i+1,j}), \quad (1)$$

where bivariate cost functions $J_{i,j}^h$ and $J_{i,j}^v$ are defined by

$$\begin{cases} J_{i,j}^h(s_1, s_2) := w_{i,j}^h d(s_1 \mathbf{v}_{i,j}, s_2 \mathbf{v}_{i,j+1}) \\ J_{i,j}^v(s_1, s_2) := w_{i,j}^v d(s_1 \mathbf{v}_{i,j}, s_2 \mathbf{v}_{i+1,j}) \end{cases} \quad (2)$$

with the use of a *distance* $d: \mathcal{V} \times \mathcal{V} \rightarrow [0, \infty)$ satisfying

$$\forall \mathbf{v}_1, \mathbf{v}_2 \quad d(\mathbf{v}_1, \mathbf{v}_2) = d(-\mathbf{v}_1, -\mathbf{v}_2) \quad (3)$$

This work was supported by JSPS KAKENHI Grant Number 17H07243.

and positive weights $w_{i,j}^h > 0$ and $w_{i,j}^v > 0$. After finding \mathbf{S}^* , the 180-degree ambiguity of $\mathbf{v}_{i,j}$ is resolved by $s_{i,j}^* \mathbf{v}_{i,j}$. \square

Remark 1 (On the Optimal Solutions of Problem 1): In Problem 1, there are at least two minimizers of (1) because $J(\mathbf{S}) = J(-\mathbf{S})$ holds for any $\mathbf{S} \in \{-1, +1\}^{m \times n}$ from (2) and (3). As a result, we need other information to judge which minimizer should be used for the 180-degree ambiguity resolution. \square

Problem 1 is designed on the basis of the idea that the true vector field varies smoothly between many neighboring pairs. In [15], [16], it is proven that the cost function J in (1) is *non-submodular*. Therefore, Problem 1 cannot be solved by graph cuts, differently from 2D phase unwrapping [20]–[24] which resolves the integer ambiguity at 2D lattice points. As approximate solvers for Problem 1, the path-following method [12], the quadratic pseudo-Boolean optimization based method [15], [16], and the Jacobi relaxation method [18], [19] are proposed.

In this paper, as a novel approximate solver for Problem 1, we propose a branch cut type algorithm in Section III, which is inspired by Goldstein’s combinatorial approach to 2D phase unwrapping [20] in Section II. Numerical experiments in Section IV demonstrate the effectiveness of the proposed method in application to the single-frame fringe projection profilometry by comparison with the existing path-following method [12]. Finally, in Section V, we conclude this paper.

Notation: Let \mathbb{Z} and \mathbb{R} be respectively the set of all integers and real numbers. Boldface small letters express vectors, and boldface capital letters express matrices. The ℓ_2 norm of $\mathbf{x} := (x_1, x_2, \dots, x_n)^T \in \mathbb{R}^n$ is denoted by $\|\mathbf{x}\|_2 := \sqrt{\sum_{i=1}^n |x_i|^2}$. In what follows, we define $(x_i, y_j) := (i, j)$ ($i = 1, 2, \dots, m$ and $j = 1, 2, \dots, n$), and for any function f define on $\Omega := [x_1, x_m] \times [y_1, y_n]$, we use the notation $f_{i,j} := f(x_i, y_j)$.

II. GOLDSTEIN’S BRANCH CUT FOR PHASE UNWRAPPING

2D phase unwrapping [20]–[24] is a reconstruction problem of an unknown continuous phase function $\phi: \Omega \rightarrow \mathbb{R}$ from its wrapped samples

$$\phi_{i,j}^W := W(\phi_{i,j}) \in (-\pi, \pi], \quad (4)$$

where $W: \mathbb{R} \rightarrow (-\pi, \pi]$ is the *wrapping operator* defined by

$$\forall \varphi \in \mathbb{R} \quad \exists z \in \mathbb{Z} \quad \varphi = W(\varphi) + 2\pi z \quad \text{and} \quad W(\varphi) \in (-\pi, \pi].$$

The continuous phase $\phi_{i,j}$ and the wrapped sample $\phi_{i,j}^W$ are respectively called the *unwrapped phase* and the *wrapped phase*. 2D phase unwrapping is important for signal and image pro-

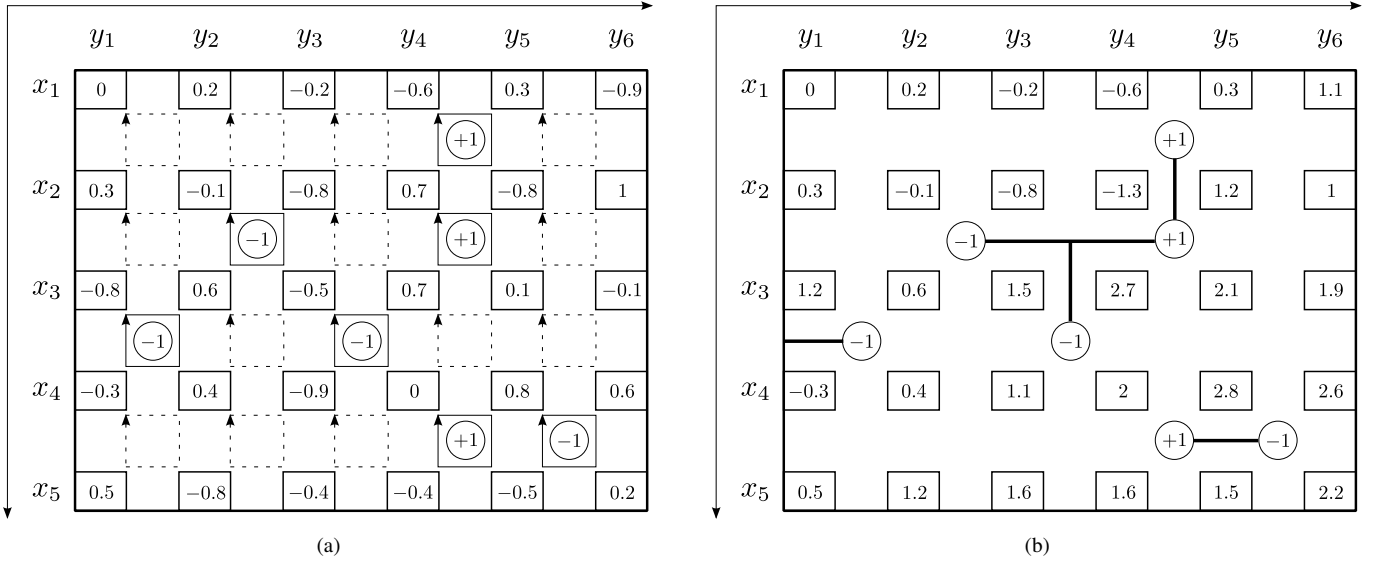


Fig. 1. Illustration of the idea of Goldstein's branch cut [20] for 2D phase unwrapping: (a) detection of every closed loop having a nonzero residue $r_{i,j} = \pm 1$ in (7) from given normalized wrapped phase $\phi_{i,j}^W/\pi$ ($i = 1, 2, \dots, 5$ and $j = 1, 2, \dots, 6$) and (b) construction of branches and the corresponding normalized unwrapped phase $\phi_{i,j}/\pi$ ($i = 1, 2, \dots, 5$ and $j = 1, 2, \dots, 6$).

cessing applications, e.g., *terrain height estimation* and *landslide identification* by interferometric synthetic aperture radar (InSAR) [25]–[30], *seafloor depth estimation* by interferometric synthetic aperture sonar (InSAS) [31]–[34], *three-dimensional (3D) shape measurement* by fringe projection [35]–[38] or X-ray [39]–[42], and *water/fat separation* in magnetic resonance imaging (MRI) [43]–[46].

In noise-free situations, we only have to resolve the integer ambiguity $z_{i,j} \in \mathbb{Z}$ of the wrapped phase $\phi_{i,j}^W$ in (4) such that

$$\phi_{i,j} = \phi_{i,j}^W + 2\pi z_{i,j} \quad (5)$$

at each lattice point. All commonly used 2D phase unwrapping algorithms assume $\phi_{i,j+1} - \phi_{i,j} = W(\phi_{i,j+1}^W - \phi_{i,j}^W) \in (\pi, \pi]$ and $\phi_{i+1,j} - \phi_{i,j} = W(\phi_{i+1,j}^W - \phi_{i,j}^W) \in (\pi, \pi]$ for most (i, j) , and (approximately) solve the following optimization problem.

Problem 2 (A Combinatorial Optimization Problem on Integer Matrices for 2D Phase Unwrapping): Find a integer matrix $\mathbf{Z}^* := (z_{i,j}^*) \in \mathbb{Z}^{m \times n}$ which minimizes

$$\begin{aligned} \Lambda(\mathbf{Z}) := & \sum_{i=1}^m \sum_{j=1}^{n-1} \tilde{w}_{i,j}^h |\phi_{i,j+1} - \phi_{i,j} - W(\phi_{i,j+1}^W - \phi_{i,j}^W)|^p \\ & + \sum_{i=1}^{m-1} \sum_{j=1}^n \tilde{w}_{i,j}^v |\phi_{i+1,j} - \phi_{i,j} - W(\phi_{i+1,j}^W - \phi_{i,j}^W)|^p \quad (6) \end{aligned}$$

subject to (5), where $p \geq 0$ and $\tilde{w}_{i,j}^h, \tilde{w}_{i,j}^v > 0$. After finding \mathbf{Z}^* , the unwrapped phase is given by $\phi_{i,j} = \phi_{i,j}^W + 2\pi z_{i,j}^*$. \square

If $p \geq 1$, then the cost function Λ in (6) is *submodular*, and hence Problem 2 can be solved by graph cuts [23]. In case of $p \in [0, 1]$, Goldstein et al. proposed the following *branch cut* algorithm [20] as an approximate solver for Problem 2. This algorithm is known as one of the path-following methods [22].

1. First, on Ω , detect every closed loop $\text{CL}_{i,j} := ((x_i, y_j) \rightarrow (x_i, y_{j+1}) \rightarrow (x_{i+1}, y_{j+1}) \rightarrow (x_{i+1}, y_j) \rightarrow (x_i, y_j))$ hav-

ing a nonzero *residue* by discretized contour integrals

$$\begin{aligned} r_{i,j} := & \frac{1}{2\pi} \left(W(\phi_{i,j+1}^W - \phi_{i,j}^W) + W(\phi_{i+1,j+1}^W - \phi_{i,j+1}^W) \right. \\ & \left. - W(\phi_{i+1,j+1}^W - \phi_{i+1,j}^W) - W(\phi_{i+1,j}^W - \phi_{i,j}^W) \right) \\ = & \begin{cases} 0 & (\text{CL}_{i,j} \text{ has no residue}), \\ \pm 1 & (\text{CL}_{i,j} \text{ has a positive/negative residue}). \end{cases} \quad (7) \end{aligned}$$

Mark the centers of such loops with ± 1 (see Fig. 1(a)).

2. Second, create *branches* by connecting the positive and negative residues (see Fig. 1(b)). Each branch is defined as a path connecting the same number of positive residues and negative residues, or connecting the residues and the outside of Ω .

3. Third, construct the unwrapped phase $\phi_{i,j}$ based on the branches by satisfying $\phi_{1,1} = \phi_{1,1}^W + 2\pi z_{1,1}$ ($z_{1,1} \in \mathbb{Z}$),

$$\phi_{i,j+1} - \phi_{i,j} = W(\phi_{i,j+1}^W - \phi_{i,j}^W) \in (\pi, \pi]$$

if there is no branch between (x_i, y_j) and (x_i, y_{j+1}) , and

$$\phi_{i+1,j} - \phi_{i,j} = W(\phi_{i+1,j}^W - \phi_{i,j}^W) \in (\pi, \pi]$$

if there is no branch between (x_i, y_j) and (x_{i+1}, y_j) . This algorithm guarantees $W(\phi_{i,j}) = \phi_{i,j}^W$ at all lattice points (x_i, y_j) (see Fig. 1(b)).

III. A BRANCH CUT TYPE ALGORITHM FOR PROBLEM 1

A. Reformulation of Problem 1

In (1), the values of $J_{i,j}^h$ and $J_{i,j}^v$ depend only sign changes between neighboring pairs $(s_{i,j}, s_{i,j+1})$ and $(s_{i,j}, s_{i+1,j})$, respectively, from (2) and (3). For each sign matrix $\mathbf{S} = (s_{i,j}) \in \{-1, +1\}^{m \times n}$, we define sign change matrices $\mathbf{C}_h = (c_{i,j}^h) \in \{0, 1\}^{m \times (n-1)}$ and $\mathbf{C}_v = (c_{i,j}^v) \in \{0, 1\}^{(m-1) \times n}$ by

$$c_{i,j}^h := \begin{cases} 0 & \text{if } s_{i,j+1} = s_{i,j}, \\ 1 & \text{if } s_{i,j+1} = -s_{i,j}, \end{cases} \quad (8)$$

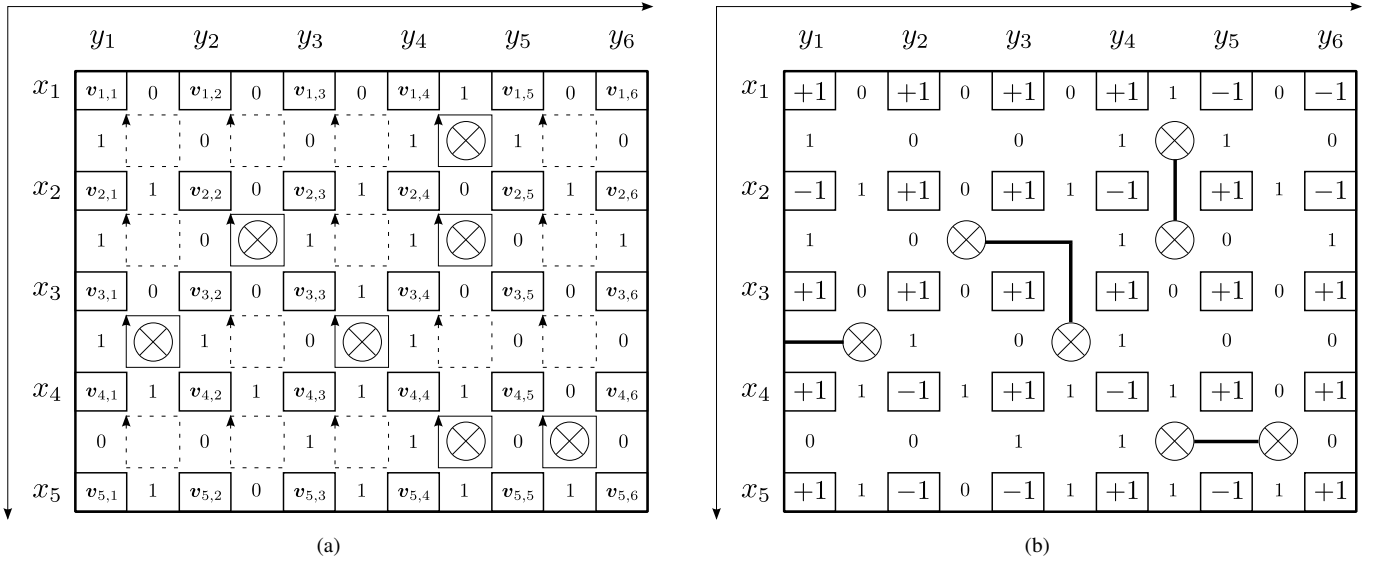


Fig. 2. Illustration of the idea of the proposed branch cut type sign estimator: (a) detection of every closed loop satisfying (12) by using the locally ideal sign changes $c_{i,j}^{h,\min}$ and $c_{i,j}^{h,\min}$ computed from $v_{i,j}$ ($i = 1, 2, \dots, 5$ and $j = 1, 2, \dots, 6$) and (b) constructions of branches, sign changes $c_{i,j}^h$ and $c_{i,j}^v$, and the corresponding signs $s_{i,j}$ ($i = 1, 2, \dots, 5$ and $j = 1, 2, \dots, 6$).

and

$$c_{i,j}^v := \begin{cases} 0 & \text{if } s_{i+1,j} = s_{i,j}, \\ 1 & \text{if } s_{i+1,j} = -s_{i,j}. \end{cases} \quad (9)$$

Moreover, define univariate functions $\hat{J}_{i,j}^h : \{0, 1\} \rightarrow [0, \infty)$ and $\hat{J}_{i,j}^v : \{0, 1\} \rightarrow [0, \infty)$ by

$$\begin{cases} \hat{J}_{i,j}^h(0) := J_{i,j}^h(1, 1) - \min \{J_{i,j}^h(1, 1), J_{i,j}^h(1, -1)\}, \\ \hat{J}_{i,j}^h(1) := J_{i,j}^h(1, -1) - \min \{J_{i,j}^h(1, 1), J_{i,j}^h(1, -1)\}, \end{cases}$$

and

$$\begin{cases} \hat{J}_{i,j}^v(0) := J_{i,j}^v(1, 1) - \min \{J_{i,j}^v(1, 1), J_{i,j}^v(1, -1)\}, \\ \hat{J}_{i,j}^v(1) := J_{i,j}^v(1, -1) - \min \{J_{i,j}^v(1, 1), J_{i,j}^v(1, -1)\}. \end{cases}$$

Then, we can reformulate Problem 1 into Problem 3 below.

Problem 3 (A Combinatorial Optimization Problem on Sign Change Matrices for 180-Degree Ambiguity Resolution): Find $(\mathbf{C}_h^*, \mathbf{C}_v^*) \in \{0, 1\}^{m \times (n-1)} \times \{0, 1\}^{(m-1) \times n}$ which minimizes

$$\hat{J}(\mathbf{C}_h, \mathbf{C}_v) := \sum_{i=1}^m \sum_{j=1}^{n-1} \hat{J}_{i,j}^h(c_{i,j}^h) + \sum_{i=1}^{m-1} \sum_{j=1}^n \hat{J}_{i,j}^v(c_{i,j}^v) \quad (10)$$

subject to

$$c_{i,j}^h \oplus c_{i,j+1}^v \oplus c_{i+1,j}^h \oplus c_{i,j}^v = 0 \quad (11)$$

for all $i = 1, 2, \dots, m-1$ and $j = 1, 2, \dots, n-1$, where \oplus denotes the *exclusive disjunction*, i.e., $0 \oplus 0 = 1 \oplus 1 = 0$ and $0 \oplus 1 = 1 \oplus 0 = 1$ hold. After finding $(\mathbf{C}_h^*, \mathbf{C}_v^*)$, the corresponding sign matrix \mathbf{S}^* can be computed (see Section III-B). The 180-degree ambiguity of $v_{i,j}$ is resolved by $s_{i,j}^* v_{i,j}$. \square

Remark 2 (On the Costs and the Constraint of Problem 3): In (10), the original costs $J_{i,j}^h$ and $J_{i,j}^v$ in (1) are replaced with the new ones $\hat{J}_{i,j}^h$ and $\hat{J}_{i,j}^v$. The constraint in (11) is necessary to guarantee the existence of the corresponding sign matrix \mathbf{S} which satisfies (8) and (9). \square

B. The Proposed Branch Cut Algorithm for Problem 3

To approximately solve Problem 3, we propose the following branch cut type algorithm, which consists of steps similar to *residue detection*, *branch construction*, and *path integration* steps of Goldstein's branch cut [20] in Section II. In the following, we suppose $\hat{J}_{i,j}^h(0) \neq \hat{J}_{i,j}^h(1)$ and $\hat{J}_{i,j}^v(0) \neq \hat{J}_{i,j}^v(1)$ for all (i, j) . Then, we define the *locally ideal sign changes* by

$$c_{i,j}^{h,\min} := \operatorname{argmin}_{c \in \{0,1\}} \hat{J}_{i,j}^h(c) \quad \text{and} \quad c_{i,j}^{v,\min} := \operatorname{argmin}_{c \in \{0,1\}} \hat{J}_{i,j}^v(c).$$

The proposed branch cut type algorithm is based on the idea that $c_{i,j}^{h,*} = c_{i,j}^{h,\min}$ and $c_{i,j}^{v,*} = c_{i,j}^{v,\min}$ may hold for most (i, j) .

1. First, on Ω , detect every closed loop $\text{CL}_{i,j}$ satisfying

$$c_{i,j}^{h,\min} \oplus c_{i,j+1}^{v,\min} \oplus c_{i+1,j}^{h,\min} \oplus c_{i,j}^{v,\min} = 1. \quad (12)$$

Mark the centers of such closed loops (see Fig. 2(a)).

2. Second, create *branches* (see Fig. 2(b)). Each branch is defined as a path connecting two centers marked in the first step, or connecting one center and the outside of Ω .
3. Third, construct sign change matrices \mathbf{C}_h and \mathbf{C}_v satisfying condition (11) by defining

$$c_{i,j}^h := \begin{cases} c_{i,j}^{h,\min} & \text{if } \left\{ \begin{array}{l} \text{there is no branch between} \\ (x_i, y_j) \text{ and } (x_i, y_{j+1}), \end{array} \right. \\ c_{i,j}^{h,\min} \oplus 1 & \text{otherwise,} \end{cases}$$

and

$$c_{i,j}^v := \begin{cases} c_{i,j}^{v,\min} & \text{if } \left\{ \begin{array}{l} \text{there is no branch between} \\ (x_i, y_j) \text{ and } (x_{i+1}, y_j), \end{array} \right. \\ c_{i,j}^{v,\min} \oplus 1 & \text{otherwise.} \end{cases}$$

Construct a sign matrix \mathbf{S} corresponding to sign change matrices \mathbf{C}_h and \mathbf{C}_v by using (8) and (9) (see Fig. 2(b)).

Remark 3 (On the Optimal Branches for Solving Problem 3): From the definitions of $\hat{J}_{i,j}^h$ and $\hat{J}_{i,j}^v$, we have $\hat{J}_{i,j}^h(c_{i,j}^{h,\min}) = 0$, $\hat{J}_{i,j}^h(c_{i,j}^{h,\min} \oplus 1) = |J_{i,j}^h(1, 1) - J_{i,j}^h(1, -1)|$, $\hat{J}_{i,j}^v(c_{i,j}^{v,\min}) = 0$, and $\hat{J}_{i,j}^v(c_{i,j}^{v,\min} \oplus 1) = |J_{i,j}^v(1, 1) - J_{i,j}^v(1, -1)|$. Therefore, we can find optimal sign changes in Problem 3 by trying to construct branches which minimize

$$\sum_{(i,j) \in E_h} |J_{i,j}^h(1, 1) - J_{i,j}^h(1, -1)| + \sum_{(i,j) \in E_v} |J_{i,j}^v(1, 1) - J_{i,j}^v(1, -1)|,$$

where

$$E_h := \{(i, j) \mid \text{branch exists between } (x_i, y_j) \text{ and } (x_i, y_{j+1})\}$$

and

$$E_v := \{(i, j) \mid \text{branch exists between } (x_i, y_j) \text{ and } (x_{i+1}, y_j)\}$$

are the sets which indicate the edges straddling branches. \square

IV. APPLICATION TO SINGLE-FRAME FRINGE PROJECTION PROFILOMETRY

A. 3D Measurement from a Single Fringe Image

Fringe projection is a major technique to obtain 3D surface information of fixed objects in a non-contact manner [47]–[49], and widely used in biomedical [50]–[52], industrial [53]–[55], kinematics [56], [57], and biometric [58], [59] applications. A typical fringe projection profilometry system is illustrated in Fig. 3. It consists of a projector, a camera and a digital computer. First, the projector projects sinusoidal fringe patterns generated by the digital computer, onto the object. Second, the camera records intensity images of the fringe patterns which are distorted due to the 3D surface profile of the object. Third, from the recorded images, the digital computer estimates the continuous phase distribution, i.e., the unwrapped phase which corresponds to the horizontal projector pixels by using some fringe analysis composed of *wrapped phase detection* and *2D phase unwrapping* steps. Finally, the 3D surface of the object is computed from the camera pixels and the projector pixels on the basis of triangulation.

A most popular fringe projection technique is the *phase-shifting method (PSM)* [60] because it can obtain 3D information stably from at least three simple fringe images as follows. Three fringe images I_k ($k = 1, 2, 3$), whose phases are shifted by $2\pi/3$ from each other, are given on the 2D plane Ω as

$$\begin{cases} I_1(x, y) = a(x, y) + b(x, y) \cos(\phi(x, y)), \\ I_2(x, y) = a(x, y) + b(x, y) \cos(\phi(x, y) - \frac{2\pi}{3}), \\ I_3(x, y) = a(x, y) + b(x, y) \cos(\phi(x, y) + \frac{2\pi}{3}), \end{cases} \quad (13)$$

where a is a slowly varying background illumination, b is the fringe amplitude that is also a low-frequency signal, and ϕ is the unwrapped phase to be estimated. The wrapped phase ϕ^W in (4) can be computed from

$$\begin{cases} \cos(\phi^W) = \cos(\phi) = \frac{2I_1 - I_2 - I_3}{\sqrt{(2I_1 - I_2 - I_3)^2 + 3(I_2 - I_3)^2}}, \\ \sin(\phi^W) = \sin(\phi) = \frac{\sqrt{3}(I_2 - I_3)}{\sqrt{(2I_1 - I_2 - I_3)^2 + 3(I_2 - I_3)^2}}. \end{cases}$$

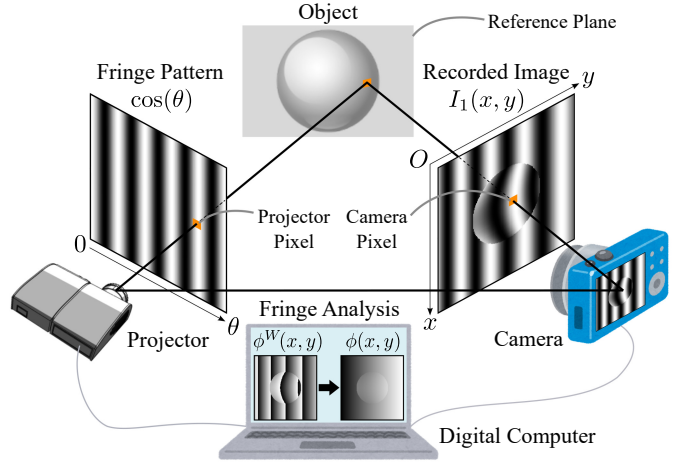


Fig. 3. Typical fringe projection profilometry system.

However, PSM requires that the physical quantities a , b and ϕ remain constant during the time needed to record the images I_k ($k = 1, 2, 3$), i.e., a , b and ϕ must be common for all indices $k = 1, 2, 3$ in (13). This condition is hardly satisfied when the measurement is for transient phenomena or the environment is hostile [15]–[17]. To deal with such situations, reconstruction of ϕ from a single fringe image I_1 in (13) has been challenged, and several phase recovery algorithms have been proposed [9]–[17]. These methods usually use a high pass filter [9] to remove the background illumination a , and use Hilbert transform [61] to normalize the fringe amplitude b . As a result, the normalized fringe image is generated from I_1 as

$$I(x, y) = \cos(\phi(x, y)) = \cos(\phi^W(x, y)) \in [-1, 1]. \quad (14)$$

From (14), we obtain the absolute value of the wrapped phase

$$|\phi^W(x, y)| = \arccos(I(x, y)) \in [0, \pi].$$

Therefore, the key of the single-frame fringe projection profilometry is estimation of the sign function in

$$\phi^W(x, y) = \text{sgn}(\phi^W(x, y)) |\phi^W(x, y)|,$$

where $\text{sgn}(t) := +1$ for $t \geq 0$ and $\text{sgn}(t) := -1$ for $t < 0$.

In the following, on the basis of the discussions in [15]–[17], we newly formulate a minimization problem for a certain energy of local change of ϕ . This energy minimization problem is a special case of Problem 1, and the optimal sign matrix $\mathbf{S}^* = (s_{i,j}^*)$ is directly used as an estimate of $\text{sgn}(\phi_{i,j}^W)$.

B. Energy Minimization for Sign Ambiguity Resolution

From (14), the fringe image gradient vector $\nabla I(x, y) := (\frac{\partial I}{\partial x}(x, y), \frac{\partial I}{\partial y}(x, y))^T$ and the unwrapped phase gradient vector $\nabla \phi(x, y) := (\frac{\partial \phi}{\partial x}(x, y), \frac{\partial \phi}{\partial y}(x, y))^T$ satisfy

$$\nabla I(x, y) = -\text{sgn}(\sin(\phi^W(x, y))) \cdot |\sin(\phi^W(x, y))| \nabla \phi(x, y).$$

Therefore, the orientation of $\nabla \phi(x, y)$ is opposite to or the same as that of $\nabla I(x, y)$ in accordance with the sign function $s(x, y) := \text{sgn}(\phi^W(x, y)) = \text{sgn}(\sin(\phi^W(x, y)))$. Based on

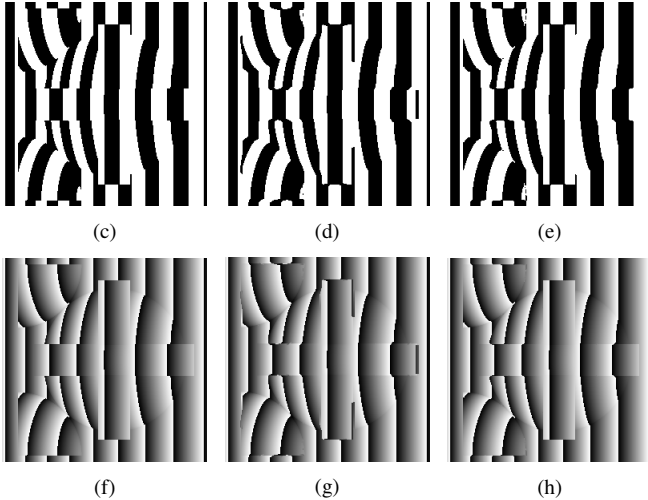
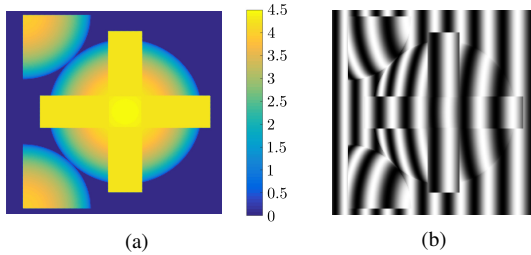


Fig. 4. Experimental results I: (a) object, (b) normalized fringe image $I_{i,j}$, (c) true signs $s_{i,j} = \text{sgn}(\phi_{i,j}^w)$ (to be estimated), (d) signs estimated by [12], (e) signs estimated by the proposed branch cut, (f) true wrapped phase $\phi_{i,j}^w$, (g) wrapped phase based on (d), and (h) wrapped phase based on (e).

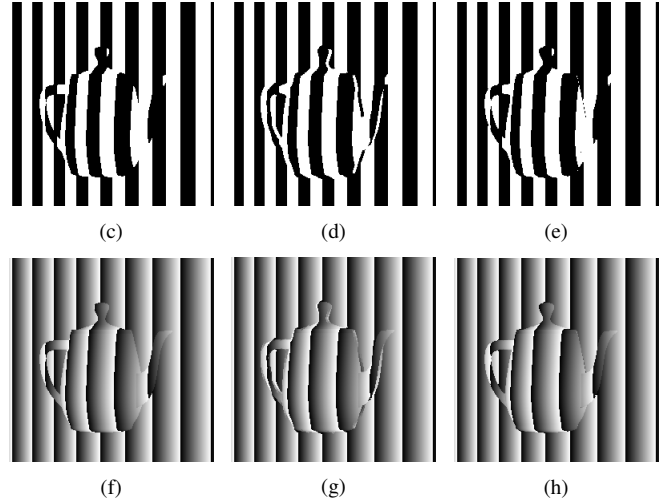
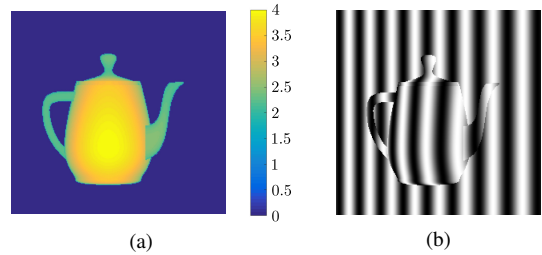


Fig. 5. Experimental results II: (a) object, (b) normalized fringe image $I_{i,j}$, (c) true signs $s_{i,j} = \text{sgn}(\phi_{i,j}^w)$ (to be estimated), (d) signs estimated by [12], (e) signs estimated by the proposed branch cut, (f) true wrapped phase $\phi_{i,j}^w$, (g) wrapped phase based on (d), and (h) wrapped phase based on (e).

the idea of *functional data analysis* [24], [62] i.e., minimization of the energy of local change of ϕ :

$$\begin{aligned} & \iint_{\Omega} \left[\left| \frac{\partial^2 \phi}{\partial x^2} \right|^2 + 2 \left| \frac{\partial^2 \phi}{\partial x \partial y} \right|^2 + \left| \frac{\partial^2 \phi}{\partial y^2} \right|^2 \right] dx dy \\ & \approx \sum_{i=1}^m \sum_{j=1}^{n-1} \|\nabla \phi(x_i, y_{j+1}) - \nabla \phi(x_i, y_j)\|_2^2 \\ & \quad + \sum_{i=1}^{m-1} \sum_{j=1}^n \|\nabla \phi(x_{i+1}, y_j) - \nabla \phi(x_i, y_j)\|_2^2, \end{aligned}$$

to estimate $s_{i,j}$, we newly introduce Problem 4 below, which is a special case of Problem 1 in Section I. Problem 4 is similar to the optimization problem in [15]–[17] for estimation of $s_{i,j}$.

Problem 4 (Approximated Energy Minimization Problem): Find $\mathbf{S}^* := (s_{i,j}^*) \in \{-1, +1\}^{m \times n}$ minimizing

$$\begin{aligned} J(\mathbf{S}) := & \sum_{i=1}^m \sum_{j=1}^{n-1} \|s_{i,j+1} \mathbf{v}_{i,j+1} - s_{i,j} \mathbf{v}_{i,j}\|_2^2 \\ & + \sum_{i=1}^{m-1} \sum_{j=1}^n \|s_{i+1,j} \mathbf{v}_{i+1,j} - s_{i,j} \mathbf{v}_{i,j}\|_2^2, \end{aligned} \quad (15)$$

where $\mathbf{v}_{i,j} := \frac{\nabla I(x_i, y_j)}{\|\nabla I(x_i, y_j)\|_2} \in \mathbb{R}^2$ is the normalized image gradient at (x_i, y_j) , and $\nabla I(x_i, y_j)$ are approximately computed by applying, e.g., the Prewitt or the Sobel operator, to I . We solve Problem 4 by using the proposed branch cut algorithm. \square

C. Numerical Experiments

We compare the effectiveness of the proposed sign estimator with that of an existing path-following sign estimator [12] for two objects shown in Figs. 4(a) and 5(a). In both experiments, we set $m = n = 256$, $a(x, y) = 2$ and $b(x, y) = 1$ for all $(x, y) \in \Omega$. We generate the normalized fringe image $I(x, y)$ by subtracting $\frac{1}{65536} \sum_{i=1}^{256} \sum_{j=1}^{256} I_1(x_i, y_j)$ from $I_1(x, y)$ followed by the normalization into $[-1, 1]$.

Figure 4(b) shows¹ the normalized fringe image $I_{i,j}$ based on the object in Fig. 4(a). Figure 4(c) shows the true signs $s_{i,j} = \text{sgn}(\phi_{i,j}^w)$, to be estimated, of the wrapped phase $\phi_{i,j}^w$ in Fig. 4(f). Figures 4(d) and 4(g) respectively depict the signs and the wrapped phase estimated by the existing method [12] using the parameters $\mu = 1$ and $\Gamma = 11$. Figures 4(e) and 4(h) respectively depict the signs and the wrapped phase estimated by the proposed branch cut, where we construct branches by repeatedly connecting the closest pair of the centers of closed loops satisfying (12). From these figures, we observe that the proposed branch cut type sign estimator achieves lower error rate ($\frac{190}{65536} \approx 0.29\%$) compared with the existing method [12] ($\frac{1053}{65536} \approx 1.61\%$) especially around the edges of the object.

Figure 5(b) shows $I_{i,j}$ for the other object (“teapot” provided in MATLAB®) in Fig. 5(a). Figure 5(c) shows the true signs $s_{i,j}$ of the wrapped phase $\phi_{i,j}^w$ in Fig. 5(f). Figures 5(d)

¹For each image in Figs. 4(b)–4(h) and 5(b)–5(h), the sample values in [Min, Max] at lattice points are rescaled into [0 (black), 255 (white)].

and 5(g) depict the signs and the wrapped phase estimated by the existing method [12]. Figures 5(e) and 5(h) depict the signs and the wrapped phase estimated by the proposed branch cut. In this experiment, the proposed sign estimator achieves again lower error rate ($\frac{141}{65536} \approx 0.22\%$) compared with the existing method ($\frac{1167}{65536} \approx 1.78\%$).

V. CONCLUSION

In this paper, for the 180-degree ambiguity resolution in 2D vector fields, we have proposed a branch cut algorithm which approximately solves Problem 1. We reformulated this combinatorial optimization problem on sign matrices into an equivalent constrained optimization problem on sign change matrices (Problem 2). Based on the idea that the optimal sign changes is the same as the locally ideal sign changes for many neighboring lattice points, we designed a branch cut type algorithm which consists of steps similar to those of Goldstein's branch cut for 2D phase unwrapping. The proposed branch cut efficiently constructs an approximate solution of the original NP-hard problem. Numerical experiments, in application to single-frame fringe projection profilometry, showed that the proposed method provides a remarkable improvement over the existing path-following method especially around the edges of objects.

REFERENCES

- [1] T. W. Gerling, "Remote sensing of the ocean-surface wind field with a scatterometer and a synthetic aperture radar," *Johns Hopkins APL Technical Digest*, vol. 6, no. 4, pp. 320–329, Oct.–Dec. 1985.
- [2] W. H. Heil, B. Cushman-Roisin, and J. J. O'Brien, "Realizing two-dimensional, continuous directed fields by vector fields and an algorithm to remove dichotomous ambiguity in a discrete field," *Mathematical and Computer Modelling*, vol. 10, no. 11, pp. 853–862, 1988.
- [3] J. J. Aly, "On the reconstruction of the nonlinear force-free coronal magnetic field from boundary data," *Solar Physics*, vol. 120, no. 1, pp. 19–48, Mar. 1989.
- [4] T. R. Metcalf, "Resolving the 180-degree ambiguity in vector magnetic field measurements: The 'minimum' energy solution," *Solar Physics*, vol. 155, no. 2, pp. 235–242, Dec. 1994.
- [5] K. D. Leka, G. Barnes, A. D. Crouch, T. R. Metcalf, G. A. Gary, J. Jing, and Y. Liu, "Resolving the 180° ambiguity in solar vector magnetic field data: Evaluating the effects of noise, spatial resolution, and method assumptions," *Solar Physics*, vol. 260, no. 1, pp. 83–108, Nov. 2009.
- [6] L. R. Benckert, "A method to resolve the 180° ambiguity in speckle photography," *Applied Optics*, vol. 30, no. 4, pp. 376–378, Feb. 1991.
- [7] M. Sjö Dahl, "Electronic speckle photography: increased accuracy by non-integral pixel shifting," *Applied Optics*, vol. 33, no. 28, pp. 6667–6673, Oct. 1994.
- [8] Z. Gao, M. Shen, H. Yu, and K. Zhang, "Simple method for simultaneously measuring the magnitude and direction of 2D in-plane displacement in white-light speckle photography," *Journal of Modern Optics*, vol. 63, no. 8, pp. 809–818, 2016.
- [9] M. Servin, J. L. Marroquin, and F. J. Cuevas, "Demodulation of a single interferogram by use of a two-dimensional regularized phase-tracking technique," *Applied Optics*, vol. 36, no. 19, pp. 4540–4548, Jul. 1997.
- [10] J. A. Quiroga, M. Servin, and F. J. Cuevas, "Modulo 2π fringe orientation angle estimation by phase unwrapping with a regularized phase tracking algorithm," *Journal of the Optical Society of America A: Optics, Image Science, and Vision*, vol. 19, no. 8, pp. 1524–1531, Aug. 2002.
- [11] C. J. Tay, C. Quan, F. J. Yang, and X. Y. He, "A new method for phase extraction from a single fringe pattern," *Optics Communications*, vol. 239, no. 4–6, pp. 251–258, Sep. 2004.
- [12] J. Villa, I. De la Rosa, G. Miramontes, and J. A. Quiroga, "Phase recovery from a single fringe pattern using an orientational vector-field-regularized estimator," *Journal of the Optical Society of America A: Optics, Image Science, and Vision*, vol. 22, no. 12, pp. 2766–2773, 2005.
- [13] H. Wang and Q. Kema, "Frequency guided methods for demodulation of a single fringe pattern," *Optics Express*, vol. 17, no. 17, pp. 15118–15127, Aug. 2009.
- [14] C. Tian, Y. Yang, D. Liu, Y. Luo, and Y. Zhuo, "Demodulation of a single complex fringe interferogram with a path-independent regularized phase-tracking technique," *Applied Optics*, vol. 49, no. 2, pp. 170–179, Jan. 2010.
- [15] D. Wu and K. L. Boyer, "Sign ambiguity resolution for phase demodulation in interferometry with application to prelens tear film analysis," in *Proceedings of IEEE Conference on Computer Vision and Pattern Recognition (CVPR'10)*, 2010, pp. 2807–2814.
- [16] D. Wu and K. L. Boyer, "Markov random field based phase demodulation of interferometric images," *Computer Vision and Image Understanding*, vol. 115, no. 6, pp. 759–770, Jun. 2011.
- [17] W. Zeng, X. Zhong, and J. Li, "Eliminating sign ambiguity for phase extraction from a single interferogram," *Optical Engineering*, vol. 52, no. 12, 7 pages, Dec. 2013.
- [18] K. Shirai, M. Okuda, and M. Ikehara, "Color-line vector field and local color component decomposition for smoothing and denoising of color images," in *Proceedings of the 21st International Conference on Pattern Recognition (ICPR'12)*, 2012, pp. 3050–3053.
- [19] M. Rizkinia, T. Baba, K. Shirai, and M. Okuda, "Local spectral component decomposition for multi-channel image denoising," *IEEE Transactions on Image Processing*, vol. 25, no. 7, pp. 3208–3218, Jul. 2016.
- [20] R. M. Goldstein, H. A. Zebker, and C. L. Werner, "Satellite radar interferometry: Two-dimensional phase unwrapping," *Radio Science*, vol. 23, no. 4, pp. 713–720, Jul./Aug. 1988.
- [21] D. C. Ghiglia and M. D. Pritt, *Two-Dimensional Phase Unwrapping: Theory, Algorithms, and Software*. New York, NY: Wiley, 1998.
- [22] L. Ying, "Phase unwrapping," in *Wiley Encyclopedia of Biomedical Engineering, 6-Volume Set*, M. Akay, Ed. New York, NY: Wiley, 2006.
- [23] J. M. Bioucas-Dias and G. Valadao, "Phase unwrapping via graph cuts," *IEEE Transactions on Image Processing*, vol. 16, no. 3, pp. 698–709, Mar. 2007.
- [24] D. Kitahara and I. Yamada, "Algebraic phase unwrapping based on two-dimensional spline smoothing over triangles," *IEEE Transactions on Signal Processing*, vol. 64, no. 8, pp. 2103–2118, Apr. 2016.
- [25] L. C. Graham, "Synthetic interferometer radar for topographic mapping," *Proceedings of the IEEE*, vol. 62, no. 6, pp. 763–768, Jun. 1974.
- [26] H. A. Zebker and R. M. Goldstein, "Topographic mapping from interferometric synthetic aperture radar observations," *Journal of Geophysical Research*, vol. 91, no. B5, pp. 4993–4999, Apr. 1986.
- [27] A. Moccia and S. Vetrilla, "A tethered interferometric synthetic aperture radar (SAR) for a topographic mission," *IEEE Transactions on Geoscience and Remote Sensing*, vol. 30, no. 1, pp. 103–109, Jan. 1992.
- [28] P. A. Rosen, S. Hensley, I. R. Joughin, F. K. Li, S. N. Madsen, E. Rodriguez, and R. M. Goldstein, "Synthetic aperture radar interferometry," *Proceedings of the IEEE*, vol. 88, no. 3, pp. 333–382, Mar. 2000.
- [29] D. Leva, G. Nico, D. Tarchi, J. Fortuny, and A. J. Sieber, "Temporal analysis of a landslide by means of a ground-based SAR interferometer," *IEEE Transactions on Geoscience and Remote Sensing*, vol. 4, no. 4, pp. 745–752, Apr. 2003.
- [30] C. Colesanti and J. Wasowski, "Investigating landslides with space-borne synthetic aperture radar (SAR) interferometry," *Engineering Geology*, vol. 88, no. 3–4, pp. 173–199, Dec. 2006.
- [31] C. de Moustier and H. Matsumoto, "Seafloor acoustic remote sensing with multibeam echo-sounders and bathymetric sidescan sonar systems," *Marine Geophysical Researches*, vol. 15, no. 1, pp. 27–42, Jan. 1993.
- [32] P. N. Denbigh, "Signal processing strategies for a bathymetric sidescan sonar," *IEEE Journal of Oceanic Engineering*, vol. 19, no. 3, pp. 382–390, Jul. 1994.
- [33] R. E. Hansen, T. O. Sæbø, K. Gade, and S. Chapman, "Signal processing for AUV based interferometric synthetic aperture sonar," in *Proceedings of MTS/IEEE OCEANS'03*, vol. 5, 2003, pp. 2438–2444.
- [34] M. P. Hayes and P. T. Gough, "Synthetic aperture sonar: A review of current status," *IEEE Journal of Oceanic Engineering*, vol. 34, no. 3, pp. 207–224, Jul. 2009.
- [35] V. Srinivasan, H. C. Liu, and M. Halioua, "Automated phase-measuring profilometry: a phase mapping approach," *Applied Optics*, vol. 24, no. 2, pp. 185–188, Jan. 1985.
- [36] H. Zhao, W. Chen, and Y. Tan, "Phase-unwrapping algorithm for the measurement of three-dimensional object shapes," *Applied Optics*, vol. 33, no. 20, pp. 4497–4500, Jul. 1994.

- [37] P. S. Huang, C. Zhang, and F. P. Chiang, "High-speed 3-D shape measurement based on digital fringe projection," *Optical Engineering*, vol. 42, no. 1, pp. 163–168, Jan. 2003.
- [38] S. Zhang, "Recent progresses on real-time 3D shape measurement using digital fringe projection techniques," *Optics and Lasers in Engineering*, vol. 48, no. 2, pp. 149–158, Feb. 2010.
- [39] P. Cloetens, W. Ludwig, J. Baruchel, D. Van Dyck, J. Van Landuyt, J. P. Guigay, and M. Schlenker, "Holotomography: Quantitative phase tomography with micrometer resolution using hard synchrotron radiation x rays," *Applied Physics Letters*, vol. 75, no. 19, pp. 2912–2914, Nov. 1999.
- [40] T. Weitkamp, A. Diaz, C. David, F. Pfeiffer, M. Stampanoni, P. Cloetens, and E. Ziegler, "X-ray phase imaging with a grating interferometer," *Optics Express*, vol. 13, no. 16, pp. 6296–6304, Aug. 2005.
- [41] A. Momose, W. Yashiro, Y. Takeda, Y. Suzuki, and T. Hattori, "Phase tomography by X-ray Talbot interferometry for biological imaging," *Japanese Journal of Applied Physics*, vol. 45, no. 6A, pp. 5254–5262, Jun. 2006.
- [42] M. Dierolf, A. Menzel, P. Thibault, P. Schneider, C. M. Kewish, R. Wepf, O. Bunk, and F. Pfeiffer, "Ptychographic X-ray computed tomography at the nanoscale," *Nature*, vol. 467, no. 7314, pp. 436–439, Sep. 2010.
- [43] G. H. Glover and E. Schneider, "Three-point Dixon technique for true water/fat decomposition with B_0 inhomogeneity correction," *Magnetic Resonance in Medicine*, vol. 18, no. 2, pp. 371–383, Apr. 1991.
- [44] J. Szumowski, W. R. Coshov, F. Li, and S. F. Quinn, "Phase unwrapping in the three-point Dixon method for fat suppression MR imaging," *Radiology*, vol. 192, no. 2, pp. 555–561, Aug. 1994.
- [45] S. M. Song, S. Napel, N. J. Pelc, and G. H. Glover, "Phase unwrapping of MR phase images using Poisson equation," *IEEE Transactions on Image Processing*, vol. 4, no. 5, pp. 667–676, May 1995.
- [46] S. Chaves, Q. S. Xiang, and L. An, "Understanding phase maps in MRI: a new outline phase unwrapping method," *IEEE Transactions on Medical Imaging*, vol. 21, no. 8, pp. 966–977, Aug. 2002.
- [47] D. Malacara, *Optical Shop Testing*, 3rd ed. New York, NY: Wiley, 2007.
- [48] S. S. Gorthi and P. Rastogi, "Fringe projection techniques: Whither we are?," *Optics and Lasers in Engineering*, vol. 48, no. 2, pp. 133–140, Feb. 2010.
- [49] S. Zhang, "Recent progresses on real-time 3D shape measurement using digital fringe projection techniques," *Optics and Lasers in Engineering*, vol. 48, no. 2, pp. 149–158, Feb. 2010.
- [50] F. Lilley, M. J. Lalor, and D. R. Burton, "Robust fringe analysis system for human body shape measurement," *Optical Engineering*, vol. 39, no. 1, pp. 187–195, Jan. 2000.
- [51] L. C. Chen and C. C. Huang, "Miniaturized 3D surface profilometer using digital fringe projection," *Measurement Science and Technology*, vol. 16, no. 5, pp. 1061–1068, Mar. 2005.
- [52] K. Genovese and C. Pappalettere, "Whole 3D shape reconstruction of vascular segments under pressure via fringe projection techniques," *Optics and Lasers in Engineering*, vol. 44, no. 12, pp. 1311–1323, Dec. 2006.
- [53] M. de Angelis, D. de Nicola, P. Ferraro, A. Finizio, and G. Pierattini, "Liquid refractometer based on interferometric fringe projection," *Optics Communications*, vol. 175, no. 4–6, pp. 315–321, Mar. 2000.
- [54] C. Quan, C. J. Tay, X. Y. He, X. Kang, and H. M. Shang, "Microscopic surface contouring by fringe projection method," *Optics and Lasers in Engineering*, vol. 34, no. 7, pp. 547–552, Oct. 2002.
- [55] J. Burke, T. Bothe, W. Osten, and C. F. Hess, "Reverse engineering by fringe projection," in *Proceedings of SPIE, Interferometry XI: Applications*, 2002, pp. 312–324.
- [56] S. Tan, D. Song, and L. Zeng, "A tracking fringe method for measuring the shape and position of a swimming fish," *Optics Communications*, vol. 173, no. 1–6, pp. 123–128, Jan. 2000.
- [57] F. Yuan, D. Song, L. Zeng, "Measuring 3D profile and position of a moving object in large measurement range by using tracking fringe pattern," *Optics Communications*, vol. 196, no. 1–6, pp. 85–91, Sep. 2001.
- [58] J. Yagnik, G. S. Siva, K. R. Ramakrishnan, and L. K. Rao, "3D shape extraction of human face in presence of facial hair: A profilometric approach," in *Proceedings of IEEE Region 10 International Conference (TENCON)*, 2005, pp. 1–5.
- [59] S. Huang, Z. Zhang, Y. Zhao, J. Dai, C. Chen, Y. Xu, E. Zhang, L. Xie, "3D fingerprint imaging system based on full-field fringe projection profilometry," *Optics and Lasers in Engineering*, vol. 52, pp. 123–130, Jan. 2014.
- [60] K. Creath, "Phase-measurement interferometry techniques," *Progress in Optics*, vol. 26, pp. 349–393, 1988.
- [61] J. A. Quiroga, J. A. Gómez-Pedrero, and Á. García-Botella, "Algorithm for fringe pattern normalization," *Optics Communications*, vol. 197, no. 1–3, pp. 43–51, Sep. 2001.
- [62] J. O. Ramsay and B. W. Silverman, *Functional Data Analysis*, 2nd ed. New York, NY: Springer, 2005.